The Effect of Structural Ordering on the Charge Storage Mechanism of p-Type Organic Electrode Materials

Brian M. Peterson,‡ Cara N. Gannett,‡ Luis Melecio-Zambrano, Brett P. Fors*, and Héctor Abruña*

Department of Chemistry, Cornell University, Ithaca, NY, USA.

ABSTRACT: Understanding the properties that govern the kinetics of charge storage will enable informed design strategies and improve the rate performance of future battery materials. Herein, we study the effects of structural ordering in organic electrode materials on the charge storage mechanism. A redox active unit, N,N'-diphenyl-phenazine, was incorporated into three materials which exhibited varying degrees of ordering. From cyclic voltammetric analysis, the crystalline small molecule exhibited diffusion-limited behavior, likely arising from structural rearrangements that occur during charge/discharge. Conversely, a branched polymer network displayed surface-controlled kinetics, attributed to the amorphous structure which enabled fast ionic transport throughout charge/discharge, unimpeded by sluggish structural rearrangements. These results suggest a method for designing new materials for battery electrodes with battery-like energy densities and pseudocapacitor-like rate capabilities.

KEYWORDS: *Energy storage, organic electrode materials, polymers, electrochemistry, batteries*

1. INTRODUCTION

Electrochemical energy storage (EES) is a key element for utilizing energy generated from renewable sources at both mobile and grid level platforms.[1] Currently, lithium-ion batteries are the most widely implemented EES system because they offer high energy densities and extended cycle lifetimes. However, there remains the challenge of designing battery systems which can be charged on the order of seconds rather than hours.[2-4] Electric vehicles need extremely fast charging capabilities to compete with the convenience of traditional combustion engine-based transportation. Charging rates can be improved by addressing the kinetic limitations arising from slow ionic diffusion through the electrode material.

To date, there have been two main approaches applied to mitigate kinetic limitations associated with ion diffusion and improve ensuing rate capabilities. These are (1) decreasing diffusional pathlength by decreasing particle size (thin films, nanowires, nanoparticles, and porous materials)[5-7] and (2) alleviating the stresses associated with ion (de)intercalation[8], with the former having been more thoroughly studied. By nanoengineering battery materials, ion diffusion pathlengths can be decreased to alleviate the dependence of charging and discharging on solid state diffusion.[9,10] However, nanomaterials introduce new challenges, including increased cost, resistivity, and surface area for undesirable side reactions.[11-13]

Alternatively, improved performance can be achieved by supporting facile ion diffusion, by one or some combination of the following: reduced strain upon intercalation, elimination of phase changes accompanying the redox reaction, the existence of multiple diffusion pathways, and the reduction of activation energy barriers to ion diffusion. Intercalation pseudocapacitors, amorphous materials, and crystalline materials with designed defects have all shown improved rate performance in half-cell experiments owing to improved kinetics attributed to the aforementioned reasons.[14-18] In all cases, when the dependence on ion diffusion has been alleviated, a more pseudocapactive response follows, as evidenced by the following features: (1) current that scales linearly with sweep rate during potential scans, (2) decreasing of the peak splitting, $\Delta E_{peak,}$ in the cyclic voltammetric (CV) response, and (3) sloping galvanostatic charge/discharge curves.

Improved ionic transport in these examples improved both the kinetics of the electrochemical reaction and the overall performance. Thus, we sought to investigate if ion transport and its electrochemical signature (pseudocapacitive or battery-type) could be controlled in organic redox active materials by tuning the morphology. While many inorganic materials have been structurally altered to exhibit pseudocapacitive behavior, there are no systematic studies on altering the structure of organic electrode materials to alleviate the kinetic limitations imposed by a diffusion-controlled charge storage mechanism. Herein, we demonstrate the ability to deliberately alter the charge storage mechanism by changing structure through the study of a common redox active unit incorporated into materials of varied morphologies.

Owing to the weaker intermolecular forces in organic compounds, compared to inorganic materials, many crystalline organic electrode materials can better tolerate the fast ion movement associated with high charge-discharge rates. Diffusion coefficients, obtained from organic-based electrodes, have exhibited orders of magnitude improvements over their crystalline inorganic counterparts.[19,20] Additionally, amorphous materials enable isotropic transport of

ions, facilitating higher rates of diffusion by an increased number of viable transport pathways.[14,15,21,22] Therefore, we sought to determine the influence of ordering in an organic structure on the charge storage mechanism of an electrode material.

For this study, N,N'-diphenyl-phenazine (Ph_2PZ) was selected as the charge storage unit for its fast and reversible electron transfer kinetics at high potentials and stable cationic and dicationic states. While the small molecule itself is soluble in battery electrolyte solutions, Ph_2PZ has demonstrated excellent performance as a charge storage unit in many different organic cathode materials.[20,23-28] By comparing an insoluble, crystalline molecule, $(Ph\text{-}PZ)_{2.5}$, and two macromolecules, poly(Ph-PZ) and poly(135Ph-PZ), with decreasing degrees of crystallinity, we were able to study the effect that ordered molecular packing imposes on the kinetics of the charge storage mechanism.

2. EXPERIMENTAL

2.1 Synthesis of $(Ph\text{-}PZ)_{2.5}$. The small molecule analogue $(Ph\text{-}PZ)_{2.5}$ was synthesized according to previously reported methods.[27,29] In a Schlenk tube, phenazine (1.44 g, 8.0 mmol, 1 equiv) in *o*-xylene (8 mL) was treated dropwise with phenyl lithium (6.6 mL, 12.0 mmol, 1.5 equiv) as a 1.8 M solution in dibutyl ether at room temperature. The reaction was stirred magnetically over 4 hours. The reaction was quenched by the addition of deoxygenated water. The organic layer was canula transferred to a second Schlenk flask containing sodium sulfate and allowed to dry for 30 min. 5 mL of this solution containing 5-phenyl-5,10-dihydrophenazine (approximately 2.7 mmol, 2.7 equiv) was transferred via syringe to a Schlenk tube containing 1,4-dibromobenzene (236 mg, 1.0 mmol, 1 equiv), sodium *tert*-butoxide (317 mg, 3.3 mmol, 3,3 equiv), RuPhos Pd G2 (12 mg, 0.015 mmol, 0.02 equiv), and RuPhos ligand (7 mg, 0.015 mmol, 0.02 equiv). The reaction was stirred at 110 °C for 16 hours. The reaction was cooled to room temperature and filtered. The precipitant was washed with hot toluene (20 mL), the filtrate was combined, passed through a silica plug and concentrated under vacuum. The product was taken up into toluene and precipitated with hexanes, yielding 74 mg of pale yellow product. ^{1}H NMR (500 MHz, C_5D_5N) δ 7.74 (s, 4H), 7.66-7.60 (m, 4H), 7.51-7.40 (m, 6H), 6.47-6.39 (m, 8H), 6.09-6.03 (m, 4H), 5.89-4.83 (m, 4H). IR (ATR, cm^{-1}): ν = 2925, 1604, 1590, 1559, 1476, 1453, 1337, 1281, 1264, 1157, 1058, 1014, 878, 834, 727, 698, 616, 550.

2.2 Synthesis of poly(Ph-PZ). The poly(Ph-PZ) macromolecule was synthesized according to previously reported methods, with minor modification.[20] 5,10-dihydrophenazine (273 mg, 1.5 mmol, 1 equiv), 1,4-dibromobenzene (354 mg, 1.5 mmol, 1 equiv), sodium *tert*-butoxide (317 mg, 3.3 mmol, 2.2 equiv), RuPhos Pd G2 (11 mg, 0.015 mmol, 0.01 equiv), and RuPhos ligand (7 mg, 0.015 mmol, 0.01 equiv) were charged to a Schlenk tube. A nitrogen atmosphere was established and toluene (5 mL) was added. The reaction was stirred at 110 °C for 16 hours. The reaction was cooled, suspended in dichloromethane (100 mL), and washed with water (100 mL) five times, or until all sodium bromide was removed by powder XRD. After filtration, the polymer was dried under vacuum at 65 °C, yielding a light brown powder (360 mg). IR (ATR, cm^{-1}): ν = 3056, 1605, 1501, 1478, 1455, 1329, 1261, 1158, 1061, 1015, 924, 817, 723, 619, 562. Elemental Anal. Found: C, 81.49; H, 4.61; N, 10.28; Br, 0.97.

2.3 Synthesis of poly(135Ph-PZ). 5,10-dihydrophenazine (273 mg, 1.5 mmol, 1 equiv), 1,3,5-tribromobenzene (315 mg, 1.0 mmol, 0.66 equiv), sodium *tert*-butoxide (346 mg, 3.6 mmol, 2.4 equiv), RuPhos Pd G2 (16 mg, 0.02 mmol, 0.01 equiv), and RuPhos ligand (9.3 mg, 0.02 mmol, 0.01 equiv) were charged to a Schlenk tube. A nitrogen atmosphere was established and toluene (5 mL) was added. The reaction was stirred at 110 °C for 16 hours. The reaction was cooled, suspended in dichloromethane (100 mL), and washed with water (100 mL) five times, or until all sodium bromide was removed by powder XRD. After filtration, the polymer was dried under vacuum at 65 °C, yielding a brown powder (312 mg) IR (ATR, cm^{-1}): ν = 3056, 1574, 1478, 1439, 1319, 1279, 1245, 1144, 1012, 931, 846, 733, 704, 621, 566. Elemental Anal. Found: C, 77.87; H, 4.28; N, 10.90; Br, 2.01.

2.4 Characterization. XRD measurements were obtained on a Rigaku Ultima IV X-ray diffractometer at a 40 kV operating voltage and 44 mA current, scanning at 2.0 °/min. Infrared spectra (IR) were recorded on a Bruker Tensor II with an ATR attachment (Figure S1). Differential scanning calorimetry (DSC) measurements were acquired on a TA Instruments Q1000 with a heat/cool/heat cycle at 20 °C/min when heating and 10 °C/min when cooling (Figure S2). Surface area measurements were acquired with a Micromeritics 3-Flex gas sorption analyzer. Imaging was done by scanning electron microscopy (SEM) with a Zeiss Gemini 500. The materials were imaged after dispersion onto a clean silicon wafer substrate or as the assembled cathode composite using a working voltage of 1.0 keV and a 20.0 μm aperture. Signal detection was done by mixing a high efficiency secondary electron detector with an in-lens detector.

2.5 Electrochemical Testing. To prepare the Ph_2PZ-based electrodes, a composite was made by mixing 60 % active material, 15% Super P Carbon, 15% CMK-3 mesoporous carbon, and 10% poly(vinylidene fluoride) (PVDF) (percentages by weight) in *N*-methyl-2-pyrrolidone. The homogeneous mixture was spread using the doctor blade method onto a carbon paper current collector and dried in a vacuum oven for 2 hours at 60 °C and then 110 °C overnight. The coin cells were assembled in an argon filled glovebox with less than 0.50 ppm O_2. A CR 2032 coin-type cell was assembled with a Li metal disk as the anode, a dried glass microfiber filter as the separator, and 1 M $LiPF_6$ in EC/DEC (1:1 by volume) as the electrolyte solution. A Bio-Logic SP-150 potentiostat was used for cyclic voltametric measurements. Galavanostatic charge/discharge and galvanostatic intermittant titration technique (GITT) experiments were conducted on a Neware battery test station.

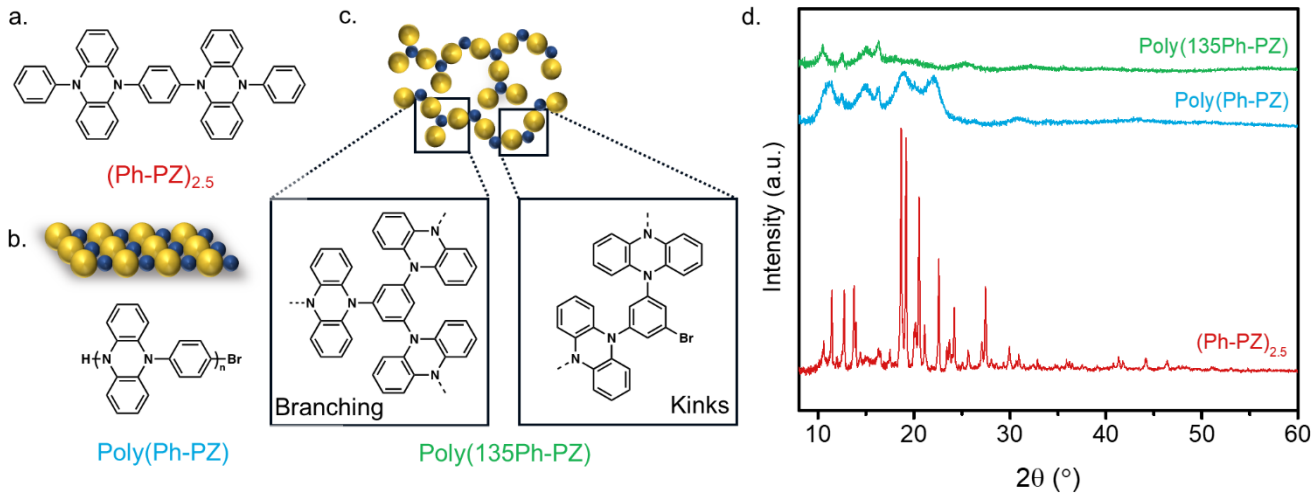

Figure 1. Schematic representations of the chemical structures of (a) $(Ph\text{-}PZ)_{2.5}$, (b) poly(Ph-PZ), and (c) poly(135Ph-PZ). (d) XRD spectra corresponding to the structures of the materials in (a-c).

3. RESULTS AND DISCUSSION

The chemical structures of the three materials investigated are shown schematically in Figures 1a-c. The NMR results for $(Ph\text{-}PZ)_{2.5}$ were in good agreement with previous reports.[24,26] The three materials displayed varying degrees of crystallinity owing to the size of the molecules and the presence/absence of branching in the macromolecules. The XRD spectra of the three materials are shown in Figure 1d. The diffraction pattern of $(Ph\text{-}PZ)_{2.5}$ confirms the crystalline nature of the small molecule. The linear polymer, poly(Ph-PZ), exhibited four peaks at low angles, suggesting the presence of strongly ordered aggregates of the polymer chains. The two broad peaks at 19 and 22°, correspond to d spacings of 4.7 and 4.0 Å, respectively, common for π stacking interactions, and are thus attributed to π–π stacking of the polymer chains.[26] Unlike the linear poly(Ph-PZ), poly(135Ph-PZ) contains 1,3,5 substitution about phenylene linkers, generating kinks and branches along the polymer chain (Figure S3). This regio-irregularity can be expected to disrupt short-range ordering and π–π stacking. The expected disruption of π–π stacking is supported by the disappearance of the peaks at 19 and 22° in the powder diffraction pattern of poly(135Ph-PZ). Armed with three materials containing Ph_2PZ, one crystalline and two amorphous with varied degrees of short-range ordering, we were equipped to probe the influence of crystallinity on the electrochemical signature of each material.

Charge storage in the Ph_2PZ unit occurs by two discrete one electron oxidations at 3.2 V and 4.0 V vs. Li/Li^+ (Figure S4).[20,26] During the charging process, Ph_2PZ is oxidized (to the cation radical) and anions present in the electrolyte solution diffuse through the material to charge compensate the electron-deficient material. The electrochemical properties of each material were determined from composites in a coin-type cell configuration. Figure 2 shows the cyclic voltammograms for each of the materials when scanned at 0.25 mV s^{-1}.

A large ΔE_{pk} is observed for both redox couples of the crystalline $(Ph\text{-}PZ)_{2.5}$, even at slow scan rates. Peak splitting values between the neutral and singly-oxidized molecule, and the singly-oxidized and dicationic molecule were 210 mV and 250 mV, respectively. A large difference in the anodic and cathodic peak potentials corresponds to a kinetic barrier between the oxidized and reduced species. This likely arises from structural changes occurring in $(Ph\text{-}PZ)_{2.5}$ to relieve the strain arising from the insertion/removal of counterions (Figure S5). Structural changes can be accompanied by volumetric expansion or contraction during charge/discharge and can adversely affect device cyclability. At 0.05 mV s^{-1}, the half-height peak widths ($\Delta E_{1/2}$'s) of $(Ph\text{-}PZ)_{2.5}$ ranged from 36 to 48 mV (Table 1). Narrow $\Delta E_{1/2}$ values (90.6 mV/n for the case of no interactions) like these are attributed to attractive interactions between redox centers, often associated with nucleation processes and phase changes.[30]

The $\Delta E_{1/2}$'s from the redox events in the polymers increase as crystallinity decreases. Broadening of the $\Delta E_{1/2}$ beyond 90.6 mV can be attributed to repulsive interactions between the redox centers. Additionally, polymers are expected to have greater spatial variation than crystalline small molecules, and therefore, electron density near the Ph_2PZ unit can vary more significantly and result in further peak broadening. The $\Delta E_{1/2}$'s of poly(Ph-PZ) fall between 60.4 – 252 mV. The first oxidation of poly(Ph-PZ) exhibits the smallest $\Delta E_{1/2}$ value (60.4 mV), more similar to (Ph-

Table 1. Half-height peak widths, $\Delta E_{1/2}$, at 0.05 mV s^{-1} [a]

Materials	Peak 1, anodic	Peak 1, cathodic	Peak 2, anodic	Peak 2, cathodic
$(Ph\text{-}PZ)_{2.5}$	40.2	48.1	43.1	36.3
Poly(Ph-PZ)	60.4	116	252	91.3
Poly(135Ph-PZ)	350	405	394	484

[a] $\Delta E_{1/2}$ values in mV.

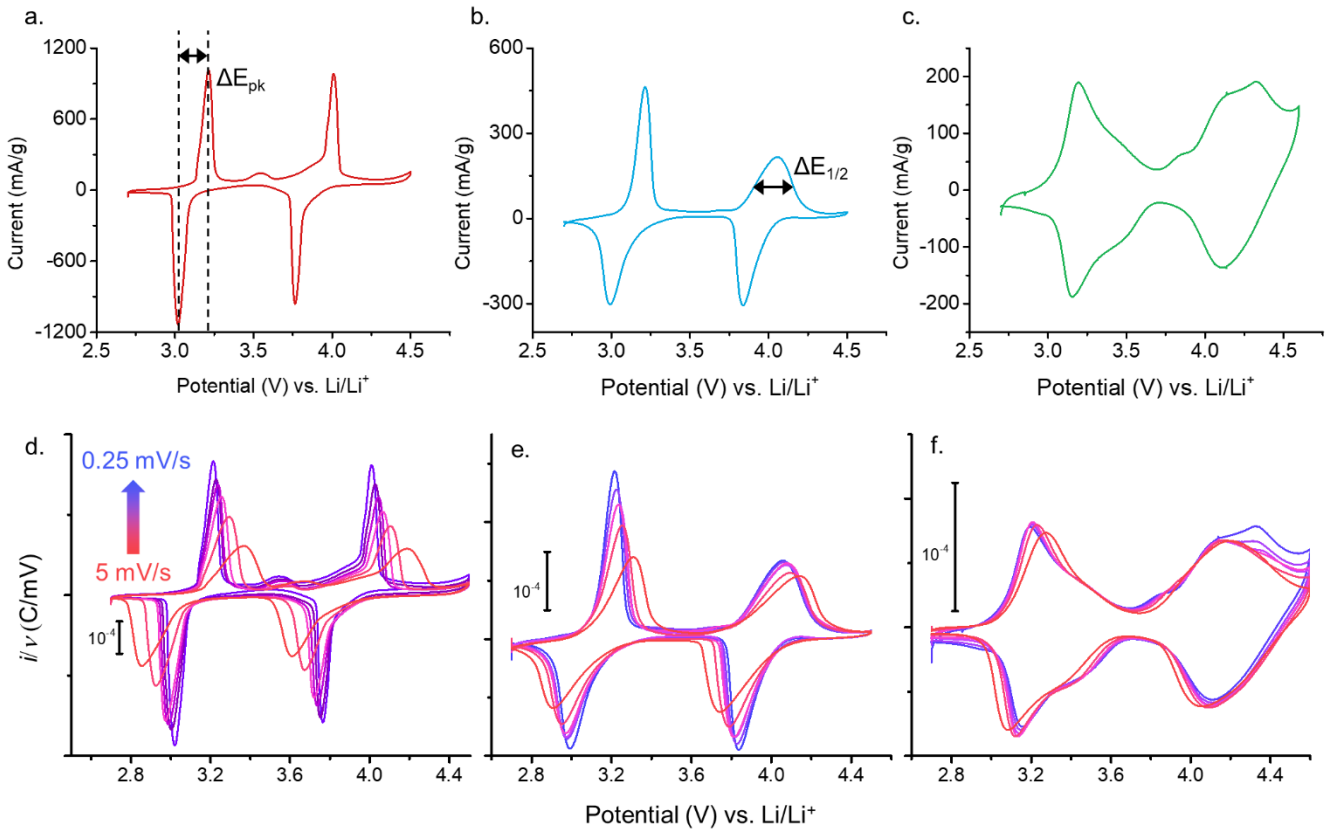

Figure 2. CV profiles with current normalized to the mass of active material at 0.25 mV s^{-1} for (a) $(Ph\text{-}PZ)_{2.5}$, (b) poly(Ph-PZ), and (c) poly(135Ph-PZ). An example of ΔE_{pk} and $\Delta E_{1/2}$ demonstrated in part (a) and (b), respectively. Cyclic voltammograms with current normalized to sweep rate for (d) $(Ph\text{-}PZ)_{2.5}$, (e) poly(Ph-PZ), and (f) poly(135Ph-PZ). The sweep rate increases from blue to red as follows: 0.25 mV s^{-1}, 0.5 mV s^{-1}, 0.75 mV s^{-1}, 1 mV s^{-1}, 2 mV s^{-1}, and 5 mV s^{-1}.

$PZ)_{2.5}$. Poly(135Ph-PZ) exhibited $\Delta E_{1/2}$'s ranging from 350 to 484 mV. The peak width is also expected to increase in poly(135Ph-PZ) due to chemically distinct redox centers at kinks and branching events, yielding a distribution of E^o values throughout the material (redox heterogeneity)[31]. We attribute a degree of this increase in $\Delta E_{1/2}$ to the disruption of the ordered domains and the stereoregularity of the redox centers through the incorporation of branching into the polymer.

The peak splitting of poly(135Ph-PZ) was significantly smaller than for either $(Ph\text{-}PZ)_{2.5}$ or poly(Ph-PZ), approaching 0 mV in the second redox couple. With fewer crystalline domains, the energetic cost of ion pairing is alleviated, phase transitions are minimized, and the kinetics of redox events are enhanced. The smaller peak splitting further indicates a redox reaction not limited by ion diffusion. When redox reactions are not limited by ion diffusion, they exhibit surface-controlled kinetics and give rise to pseudocapacitive behaviors.

Monitoring the current response over a range of scan rates yields a better understanding of the charge storage mechanism and the limiting processes in these materials. Redox reactions limited by semi-infinite linear diffusion are governed by the Randles-Sevcik relation, wherein the peak current, i_p, is proportional to the square root of the sweep rate, $\nu^{1/2}$. Alternatively, in systems where the redox reactions are surface-controlled (e.g., not limited by diffusion), i_p will scale linearly with sweep rate, ν. By plotting the current response normalized to sweep rate, we can visualize limitations in the charge storage process arising from diffusive processes (Figure 2d-f). The profile of poly(135Ph-PZ) (Figure 2f) remains relatively constant with increasing sweep rate, indicating that the reaction kinetics are not limited by ion diffusion and the processes are surface-controlled. Over this range of scan rates, neither ionic nor electronic diffusion through the material is the rate-limiting step for charge storage. In contrast, the normalized peak currents of poly(Ph-PZ) and $(Ph\text{-}PZ)_{2.5}$ decrease with increasing scan rate. This result implies that portions of the observed response are limited by diffusion. Additionally, the ΔE_{pk} and $\Delta E_{1/2}$ of poly(Ph-PZ) and $(Ph\text{-}PZ)_{2.5}$ both increase with increasing sweep rate (Figure S6). This likely indicates diffusion limitations arising from the structural changes associated with the redox reactions in these materials.

The contributions of diffusion- and surface-limited processes to the total current can be qualitatively determined using the following power law[32]:

$$i = av^b \qquad (1)$$

where a and b are adjustable parameters. A b value of 1 indicates a surface-controlled process while a b value of ½ indicates a diffusion-controlled process. The b values are determined from the slope of plots of log(peak current) vs. log(sweep rate) (Figure S7) and are presented in Figure 3a.

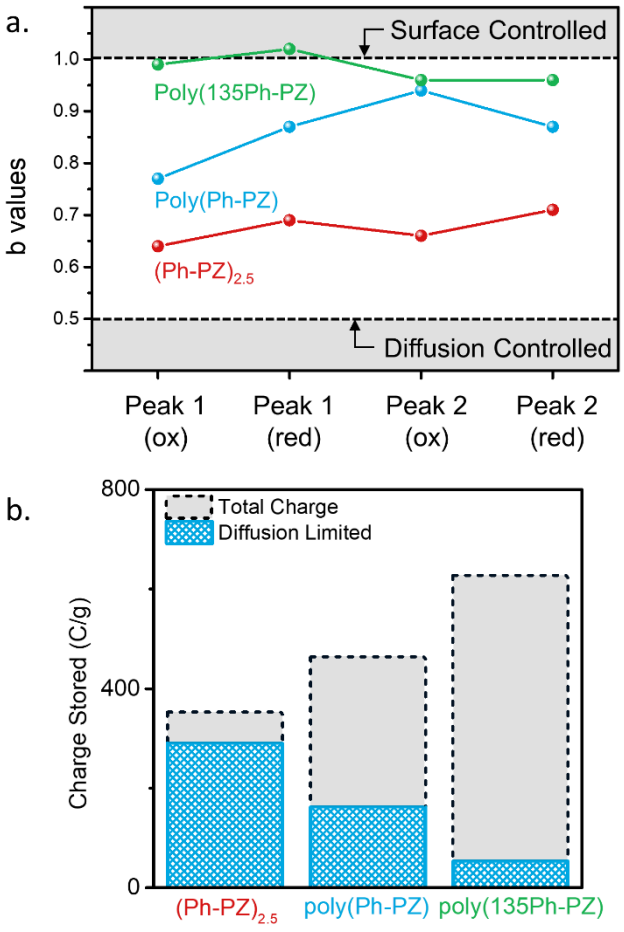

Figure 3. (a) The *b* values of $(Ph\text{-}PZ)_{2.5}$, poly(Ph-PZ), poly(135Ph-PZ) for the 0 to +1 (peak 1) and +1 to +2 (peak 2) redox couples. (b) The contribution of diffusion-limited charge to the total amount of charge stored when scanned at 0.05 mV s^{-1}.

b values closest to 0.5, illustrating the highest degree of diffusion limitations in the crystalline material. As crystallinity is disrupted in poly(Ph-PZ) and poly(135Ph- PZ), the *b* values increase. The *b* values of poly(Ph-PZ) fall between 0.77 and 0.94. Each of the redox processes in poly(135Ph-PZ) is almost entirely surface-controlled, with *b* values of approximately 1 for each of the redox peaks. Values near 1 are observed for pseudocapacitive materials. It is interesting that poly(135Ph-PZ) exhibits surface-limited behavior despite particle sizes on the order of micrometers (Figure S8) and no appreciable surface area by porosity measurements (Figure S10).

Further breakdown of the charge storage mechanism, diffusion- or surface-controlled, can be achieved with equation (2):

$$i = k_1 v + k_2 v^{1/2} \qquad (2)$$

If the total current is assumed to derive from either diffusive- or surface- controlled processes, then k_1 and k_2 are constants corresponding to the surface- controlled and diffusion-controlled currents at a given potential, respectively. Inspection of these profiles (Figure S11) illustrates a shift in the charge storage mechanism from a diffusion-controlled process to a surface-controlled process with decreased ordering in the cathode material. The charge delivered by diffusion-controlled processes relative to the total cathodic charge is depicted in the bar graph in Figure 3b. Almost all of the charge stored in $(Ph\text{-}PZ)_{2.5}$ arises from diffusion-controlled processes, except for small contributions from the electrical double layer. In stark contrast, charge storage in poly(135Ph-PZ) is dominated by surface-controlled processes.

Poly(Ph-PZ) and $(Ph\text{-}PZ)_{2.5}$ both exhibit *b* values which fall between 0.5 and 1, indicating mixed diffusion- and surface-control. Many materials display complex charge storage mechanisms which stem from concurrent diffusion-controlled and surface-controlled contributions. $(Ph\text{-}PZ)_{2.5}$ has

The galvanostatic intermittent titration technique (GITT) was used to determine the diffusion coefficients of the charge compensating ions (PF_6^-) in each material throughout the charge/discharge process (Figure 4a-c). The diffusion coefficients for each material are nearly identical at potentials where no faradaic reactions occur. However, at potentials corresponding to the faradaic events that require charge compensating ions to diffuse through the solid state, the diffusion coefficients of poly(Ph-PZ) and $(Ph\text{-}PZ)_{2.5}$ are dramatically reduced. This effect is especially pronounced with the reduction from the +1 state to neutral, where the diffusion coefficients of poly(Ph-PZ) and $(Ph\text{-}PZ)_{2.5}$ drop to 4×10^{-11} and 3×10^{-11} cm^2 s^{-1}, respectively. This decrease in the diffusion coefficients is not observed for poly(135Ph-PZ). Instead, the diffusion coefficients are maintained at ~9×10^{-10} cm^2 s^{-1} throughout discharge, representing an improvement of approximately two orders of magnitude over poly(Ph-PZ) and $(Ph\text{-}PZ)_{2.5}$. This difference is observed regardless of the charge compensating anion (Figure S12). Further, during the charging process, the diffusion coefficients of $(Ph\text{-}PZ)_{2.5}$ drop as low as 3×10^{-12} and 5×10^{-14} cm^2 s^{-1} during the first and second oxidation, respectively, while again the diffusion coefficients in poly(135Ph-PZ) remain relatively constant. This supports our conclusions from the above relationships of current with sweep rate, suggesting diffusion limitations decrease as ordering is disrupted in the electrode material. These results indicate that the disruption of ordering by the branched polymer facilitates fast ion diffusion even in instances of high ion flux during faradaic reactions.

While the diffusion coefficients corresponding to the first redox couple of poly(Ph-PZ) drop by over an order of magnitude during the faradaic events, the drop is less pronounced for the second redox couple. The first oxidation of poly(Ph-PZ) possesses the highest degree of diffusion limitations, according to the *b* value of 0.77 and supported by the decrease in the diffusion coefficients during the redox reaction observed by GITT. The diffusion limited kinetics observed for this redox couple likely arise from structural rearrangements associated with swelling the neutral polymer with counter ions and the accompanying solvent molecules. The swollen, charged polymer is better suited to support ionic transport leading to faster ionic diffusion and more pseudocapactive-like charge storage.[33]

The electrochemical signature from the galvanostatic charge/discharge (GCD) traces of $(Ph\text{-}PZ)_{2.5}$, poly(Ph-PZ), and poly(135Ph-PZ) provide further insight into the charge storage mechanism. The electrochemical signatures exhibited in GCD experiments agree with those observed by CV

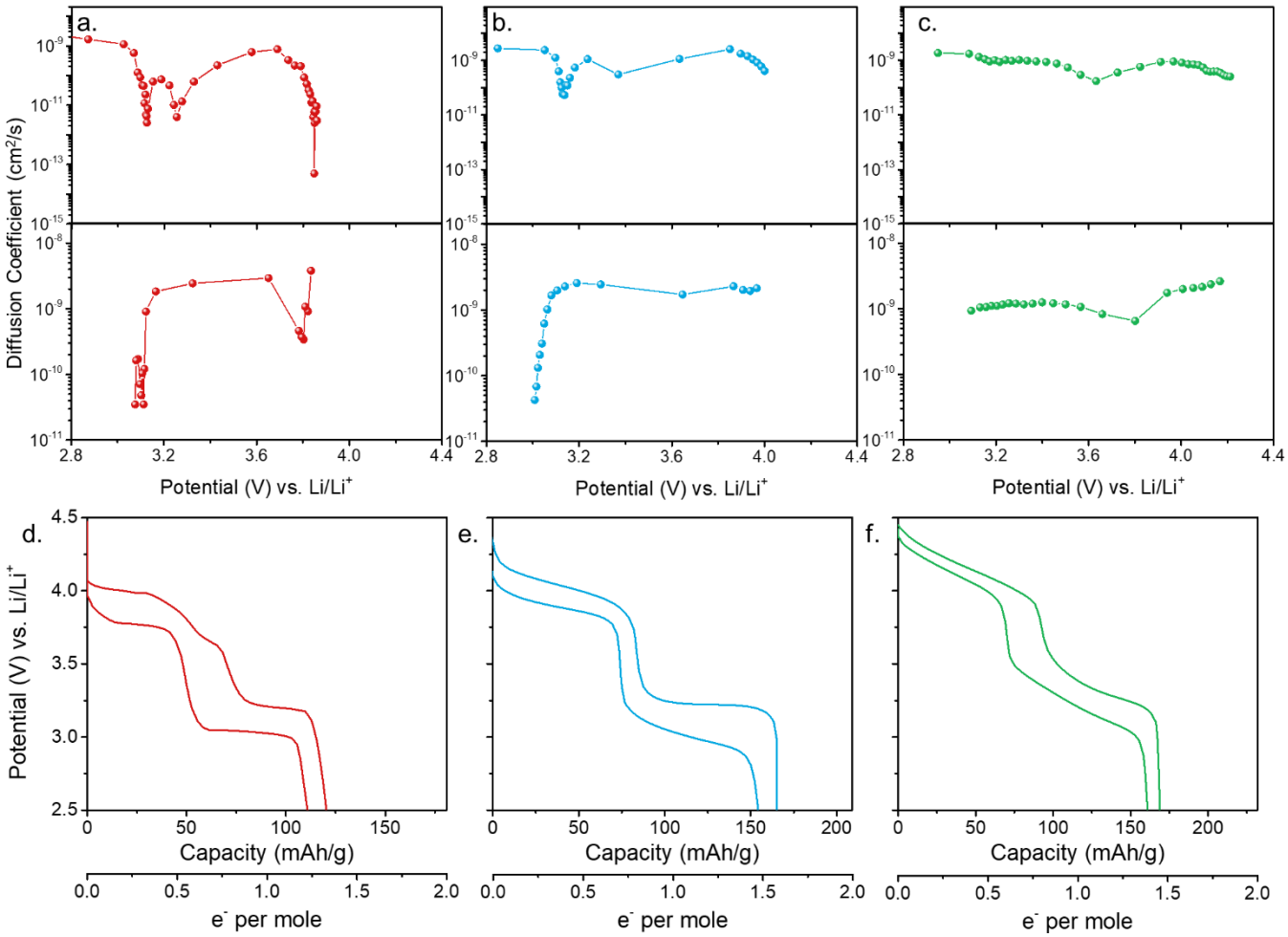

Figure 4. Diffusion coefficients from GITT during charge (top) and discharge (bottom) for (a) $(Ph\text{-}PZ)_{2.5}$, (b) poly(Ph-PZ), and (c) poly(135Ph-PZ). Galvanostatic charge discharge traces of (d) $(Ph\text{-}PZ)_{2.5}$, (e) poly(Ph-PZ), and (f) poly(135Ph-PZ).

(Figure S13 and 14). Consistent with the peak splitting in the CV experiments, the materials with less ordered domains exhibit less polarization when charged and discharged at 1 A g^{-1} (~5 C) (Figures 4d-f). The plateaus observed in the GCD profile for $(Ph\text{-}PZ)_{2.5}$ are flat, maintaining an almost constant potential through the faradaic event, while those of poly(Ph-PZ) and poly(135Ph-PZ) are increasingly sloped. This is consistent with the trends observed in the $\Delta E_{1/2}$ values of the cyclic voltametric profiles. Flat plateaus store charge at constant potentials and are characteristic of battery-type materials. Conversely, sloping plateaus and a nearly linear relationship between potential and capacity indicate an electrochemical signature of a pseudocapacitor. The sloping plateaus of poly(135Ph-PZ), along with its predominantly surface-controlled kinetics, suggest a more pseudocapacitive nature when compared to its more ordered counterparts.

In addition to its improved kinetics, poly(135Ph-PZ) delivered the highest stable capacity at 1 A g^{-1}, which is consistent with its improved theoretical capacity (C_{theor} for poly(135Ph-PZ) = 232 mAh g^{-1}) relative to the other two materials (C_{theor} for $(Ph\text{-}PZ)_{2.5}$ = 181 mAh g^{-1}, C_{theor} for poly(Ph-PZ) = 209 mAh g^{-1}). When cycled at 1 A g^{-1}, $(Ph\text{-}PZ)_{2.5}$ exhibited a steady decay in capacity and low coulombic efficiencies (~92%), which could arise from the slow dissolution of the material and/or irreversibility associated with the electrochemical reactions (Figure S15). On the other hand, the polymeric materials exhibited more stable capacities with cycling and coulombic efficiencies near unity."

4. CONCLUSIONS

Herein, we have shown that the charge storage mechanism of organic materials can be dictated through manipulation of material morphology. The redox active unit Ph_2PZ was embedded in three materials exhibiting varying degrees of ordering. Within the crystalline $(Ph\text{-}PZ)_{2.5}$, charge storage was limited by the diffusion of ions, due in large part to the energetic cost of reorganization within the crystalline domains. By decreasing the structural ordering in poly(Ph-PZ) and poly(135Ph-PZ), it is possible to alleviate diffusion-limitations associated with the charge storage mechanism. Using an amorphous structure to facilitate fast ionic diffusion, poly(135Ph-PZ) exhibited an electrochemical signature more consistent with pseudocapacitive-type energy storage. This approach to organic electrode design could be used to develop new materials with both high energy densities and excellent rate capabilities.

ASSOCIATED CONTENT

Additional characterization and electrochemical analysis can be found in the Supporting Information. This material is available free of charge via the Internet at http://pubs.acs.org.

AUTHOR INFORMATION

Corresponding Authors

Brett Fors – *Department of Chemistry and Chemical Biology, Cornell University, Ithaca, New York 14853, United States*; Email: bpf46@ cornell.edu

Héctor Abruña – *Department of Chemistry and Chemical Biology, Cornell University, Ithaca, New York 14853, United States*; Email: hda1@ cornell.edu

Author Contributions

‡These authors contributed equally to this work.

Notes

The authors declare no completing financial interest.

ACKNOWLEDGMENT

The authors would like to thank Mary Zick for performing and analyzing the BET surface area measurements and Yao Yang for performing STEM experiments. This work made use of the Cornell Center for Materials Research Shared Facilities which are supported through the NSF MRSEC program (DMR-1719875). C.N.G. and H.D.A. would like to thank the National Science Foundation Center for Synthetic Organic Electrosynthesis for funding (CHA-1740656) and Mercedes Benz for funding. L.M.Z. would like to thank the National Science Foundation Graduate Research Fellowship Program for funding (DGE-1650441).

REFERENCES

(1) Dunn, B.; Kamath, H.; Tarascon, J. Electrical energy storage for the grid: a battery of choices. *Science* **2011**, *334*(6058), 928-935.

(2) Tang, Y.; Zhang, Y.; Li, W.; Ma, B.; Chen, X. Rational material design for ultrafast rechargeable lithium-ion batteries. *Chem. Soc. Rev.* **2015**, *44*(17), 5926-5940.

(3) Choi, N.; Chen, Z.; Freunberger, S.; Ji, X.; Sun, Y.; Amine, K.; Yushin, G.; Nazar, L.; Cho, J.; Bruce, P. Challenges facing lithium batteries and electrical double-layer capacitors. *Angew. Chem., Int. Ed.* **2012**, *51*(40), 9994-10024.

(4) Augustyn, V.; Simon, P.; Dunn, B. Pseudocapacitive oxide materials for high-rate electrochemical energy storage. *Energy Environ. Sci.* **2014**, *7*(5), 1597-1614.

(5) Gogotsi, Y. What Nano Can Do for Energy Storage?. *ACS Nano* **2014**, *8*, 5369– 5371.

(6) Gogotsi, Y.; Penner, R. Energy storage in nanomaterials–capacitive, pseudocapacitive, or battery-like? *ACS Nano* **2018**, *12* (3), 2081–2083.

(7) Okubo, M.; Hosono, E.; Kim, J.; Enomoto, M.; Kojima, N.; Kudo, T.; Zhou, H.; Honma, I. Nanosize effect on high-rate Li-ion intercalation in LiCoO2 electrode. *J. Am. Chem. Soc.* **2007**, *129*(23), 7444-7452.

(8) Augustyn, V.; Come, J.; Lowe, M.; Kim, J.; Taberna, P.; Tolbert, S.; Abruña, H.; Simon, P.; Dunn, B. High-rate electrochemical energy storage through Li+ intercalation pseudocapacitance. *Nat. Mater.* **2013**, 12(6), 518-522.

(9) Ge, X.; Liu, S.; Qiao, M.; Du, Y.; Li, Y.; Bao, J.; Zhou, X. Enabling superior electrochemical properties for highly efficient potassium storage by impregnating ultrafine Sb nanocrystals within nanochannel-containing carbon nanofibers. *Angew. Chem. Int. Ed.* **2019**, *58*, 14578-14583.

(10) Xu, J.; Gu, E.; Zhang, Z.; Xu, Z.; Xu, Y.; Du, Y.; Zhu, X.; Zhou, X. Fabrication of porous Na3V2 (PO4) 3/reduced graphene oxide hollow spheres with enhanced sodium storage performance. *J. Colloid Interface Sci.* **2020**, *567*, 84-91.

(11) Kim, S.-W; Pereira, N.; Chernova, N. A.; Omenya, F.; Gao, P.; Whittingham, M. S.; Amatucci, G. G.; Su, D.; Wang, F. Structure Stabilization by Mixed Anions in Oxyfluoride Cathodes for High-Energy Lithium Batteries. *ACS Nano* **2015**, *9*, 10076– 10084.

(12) Rajput, S.; Pittman, C. U., Jr; Mohan, D. Magnetic Magnetite (Fe_3O_4) Nanoparticle Synthesis and Applications for Lead (Pb^{2+}) and Chromium (Cr^{6+}) Removal from Water. *J. Colloid Interface Sci.* **2016**, *468*, 334– 346.

(13) Jung, S.; Hwang, I.; Chang, D.; Park, K.; Kim, S.; Seong, W.; Eum, D.; Park, J.; Kim, B.; Kim, J.; Heo, J. Nanoscale Phenomena in Lithium-Ion Batteries. *Chem. Rev.* **2019**, *120,* 6684-6737.

(14) Wei, Z.; Wang, D.; Yang, X.; Wang, C.; Chen, G.; Du, F. From Crystalline to Amorphous: An Effective Avenue to Engineer High-Performance Electrode Materials for Sodium-Ion Batteries. *Adv. Mater. Interfaces* **2018**, *5* (19), 1800639.

(15) Walter, M., Kravchyk, K. V., Böfer, C., Widmer, R., & Kovalenko, M. V. Polypyrenes as High-Performance Cathode Materials for Aluminum Batteries. *Adv. Mater.* **2018**, *30*, 1705644.

(16) Chae, O.; Kim, J.; Park, I.; Jeong, H.; Ku, J.; Ryu, J.; Kang, K.; Oh, S. Reversible lithium storage at highly populated vacant sites in an amorphous vanadium pentoxide electrode. *Chem. Mater.* **2014**, *26*(20), 5874-5881.

(17) Yao, K.; Xu, Z.; Huang, J.; Ma, M.; Fu, L.; Shen, X.; Li, J.; Fu, M. Bundled Defect-Rich MoS2 for a High-Rate and Long-Life Sodium-Ion Battery: Achieving 3D Diffusion of Sodium Ion by Vacancies to Improve Kinetics. *Small* **2019**, *15*(12), 1805405.

(18) Zhang, Z.; Du, Y.; Wang, Q.C.; Xu, J.; Zhou, Y.N.; Bao, J.; Shen, J.; Zhou, X. A Yolk–Shell-Structured FePO4 Cathode for High-Rate and Long-Cycling Sodium-Ion Batteries. *Angew. Chem. Int. Ed.* **2020**, *59*(40), 17504-17510.

(19) Zhang, Y.; Sun, Y.; Du, S.; Gao, H.; Zhang, S.B. Organic salts as super-high rate capability materials for lithium-ion batteries. *Appl. Phys. Lett.* **2012**, *100*(9), 091905.

(20) Gannett, C. N.; Peterson, B. M.; Shen, L.; Seok, J.; Fors, B. P.; Abruña, H. D. Cross-linking Effects on Performance Metrics of Phenazine-Based Polymer Cathodes. *ChemSusChem* **2020**, *13*, 2428-2435.

(21) Ku, J. H.; Ryu, J. H.; Kim, S. H.; Han, O. H.; Oh, S. M. Reversible Lithium Storage with High Mobility at Structural Defects in Amorphous Molybdenum Dioxide Electrode. *Adv. Funct. Mater.* **2012**, *22* (17), 3658–3664.

(22) Uchaker, E.; Zheng, Y. Z.; Li, S.; Candelaria, S. L.; Hu, S.; Cao, G. Z. Better than Crystalline: Amorphous Vanadium Oxide for Sodium-Ion Batteries. *J. Mater. Chem. A* **2014**, *2* (43), 18208–18214.

(23) Niu, Z.; Wu, H.; Liu, L.; Dai, G.; Xiong, S.; Zhao, Y.; Zhang, X. Chain Rigidity Modification to Promote the Electrochemical Performance of Polymeric Battery Electrode Materials. *J. Mater. Chem. A* **2019**, *7* (17), 10581–10588.

(24) Dai, G.; He, Y.; Niu, Z.; He, P.; Zhang, C.; Zhao, Y.; Zhang, X.; Zhou, H. A Dual-Ion Organic Symmetric Battery Constructed from Phenazine-Based Artificial Bipolar Molecules. *Angew. Chem., Int. Ed.* **2019**, *58*(29), 9902-9906.

(25) Dai, G.; Liu, Y.; Niu, Z.; He, P.; Zhao, Y.; Zhang, X.; Zhou, H. The Design of Quaternary Nitrogen Redox Center for High-Performance Organic Battery Materials. *Matter* **2019**, *1*(4), 945-958.

(26) Obrezkov, F.; Ramezankhani, V.; Zhidkov, I.; Traven, V.; Kurmaev, E.; Stevenson, K.; Troshin, P. High-Energy and High-Power-Density Potassium Ion Batteries Using Dihydrophenazine-Based Polymer as Active Cathode Material. *J. Phys. Chem. Lett.* **2019**,*10*(18), 5440-5445.
(27) Dai, G.; Wang, X.; Qian, Y.; Niu, Z.; Zhu, X.; Ye, J.; Zhao, Y.; Zhang, X. Manipulation of conjugation to stabilize N redox-active centers for the design of high-voltage organic battery cathode. *Energy Storage Mater*. **2019**, *16*, 236-242.
(28) Lee, M.; Hong, J.; Lee, B.; Ku, K.; Lee, S.; Park, C.; Kang, K. Multi-electron redox phenazine for ready-to-charge organic batteries. *Green Chem*. **2017**, *19*(13), 2980-2985.
(29) Terada, E.; Okamoto, T.; Kozaki, M.; Masaki, M.; Shiomi, D.; Sato, K.; Takui, T.; Okada, K. Exchange Interaction of 5, 5 '-(m- and p-Phenylene) bis (10-phenyl-5, 10-dihydrophenazine) Dications and Related Analogues. *J. Org. Chem.* **2005**, *70*(24), 10073-10081.
(30) Lukatskaya, M.; Dunn, B.; Gogotsi, Y. Multidimensional materials and device architectures for future hybrid energy storage. *Nat. Commun.* **2016**, *7*(1), 1-13.
(31) Peerce, P.; Bard, A. Polymer films on electrodes: Part III. Digital simulation model for cyclic voltammetry of electroactive polymer film and electrochemistry of poly (vinylferrocene) on platinum. *J. Electroanal. Chem. Interfacial Electrochem.* **1980**,*114*(1), 89-115.
(32) Lindström, H.; Södergren, S.; Solbrand, A.; Rensmo, H.; Hjelm, J.; Hagfeldt, A.; Lindquist, S. Li+ ion insertion in TiO2 (anatase). 2. Voltammetry on nanoporous films. *J. Phys. Chem. B* **1997**, *101*(39), 7717-7722.
(33) Otero, T.; Grande, H.; Rodríguez, J. Reinterpretation of polypyrrole electrochemistry after consideration of conformational relaxation processes. *J. Phys. Chem. B* **1997**, *101*(19), 3688-3697.

Table of Contents artwork